PHYSICAL REVIEW B **96**, 100507(R) (2017)

Observation of two-dimensional superconductivity in bilayers of $BaBiO_3$ and $BaPbO_3$

B. Meir, S. Gorol, T. Kopp, and G. Hammerl
Experimental Physics VI, Center for Electronic Correlations and Magnetism, Institute of Physics, University of Augsburg, 86135 Augsburg, Germany
(Received 22 March 2017; published 21 September 2017)

Lead-doped barium bismuthate is intriguing because of its relatively high critical temperature and the nature of its superconductivity in the vicinity of a charge-density-wave-ordered topological insulator. Here we present bilayers of barium bismuthate and barium leadate showing emergent superconductivity as a function of the barium leadate top layer thickness. Magnetotransport studies allow for the characterization of the superconducting properties in these bilayers to be two-dimensional. In addition current-voltage characteristics of superconducting bilayers reveal signatures of a Berezinskiĭ-Kosterlitz-Thouless transition. The particular observed dependence of the superconducting transition temperature on the thickness of the barium leadate top layer suggests the formation of the superconducting state originating from the interface.

DOI: 10.1103/PhysRevB.96.100507

Interfaces in oxide heterostructures serve as an inexhaustible source for the creation of new electronic phases well constrained on the nanoscale [1]. Specifically, superconductivity confined to an interface is of particular importance not only because it is easy to tune by external fields but especially because the interface electron system results from an electronic reconstruction depending on bulk states with their versatile ground states [2–5]. The interface electron structure is controlled by bulk-materials properties and also by the symmetry breaking at the edge of the respective bulk materials. The prominent oxide heterostructure of the two band insulators $SrTiO_3$ (STO) and $LaAlO_3$ (LAO) hosts such an interface-confined electron liquid [6–8] showing two-dimensional (2D) superconductivity at temperatures below $\approx$300 mK [9,10]. Structural inversion symmetry breaking at the interface introduces a sizable Rashba spin-orbit coupling [11]. Also the superconducting states of cuprate bilayers have striking features: a high-T_c state confined to 2–3 nm is formed between insulating La_2CuO_4 and metallic $La_{1.55}Sr_{0.45}CuO_4$ [12], both of which are not superconducting. Moreover, heterostructures built from the insulating oxides $CaCuO_2$ and STO allow for a superconducting interface [13].

Up to now, only a few superconducting oxide interfaces have been realized, and the microscopic mechanism for the formation of a superconducting state at either heterostructure is still under debate. It is an appealing challenge to identify further superconducting bilayers because different perovskite parent compounds, notably those with intrinsic intriguing physical properties, account for novel characteristics of electronic states in proximity to the interface. For example, $BaBiO_3$ (BBO) is predicted to be a large-energy-gap topological insulator due to spin-orbit coupling (when electron doped) [14], whereas the related compound $BaPbO_3$ (BPO) is a bulk metal [15]. In fact, both BBO and BPO are expected to preserve a "hidden" topological insulator phase when electron or hole doped [16,17]. Moreover, lead-doped bulk BBO is well known to be superconducting [18]. That finding now raises the question of whether the interface region between BBO and BPO induces superconductivity that is possibly two-dimensional and just off topological surface states.

BBO crystallizes at room and low temperatures in perovskite-related monoclinic structures [19]. The underlying octahedral distortion leads to symmetric breathing-mode displacements forcing the Bi^{3+} and Bi^{5+} ions to distinct crystal sites, forming a bond-order charge-density wave (CDW) [20–23]. The charge-ordered state can be altered by, e.g., substituting the metal cations in BBO, giving rise to tremendous changes in the structural and electronic properties of this very special perovskite: in homogeneously doped bulk samples of $BaBi_{1-x}Pb_xO_3$ (BBPO) three-dimensional superconductivity is observed for doping ranges of $0.65 < x < 0.95$, with a sharp maximum superconducting transition temperature of $T_c \approx 13$ K for x near 0.75 [24–28]. The onset of superconductivity is attributed to the formation of a bimorphic phase consisting of orthorhombic and tetragonal polymorphs in BBPO [27–30]. By substituting barium with potassium, bulk samples of $Ba_{1-x}K_xBiO_3$ yield maximum critical temperatures of $T_c \approx 30$ K for a potassium concentration of $x = 0.4$ [31]. The high-T_c superconductivity of these compounds was recently linked to correlation-enhanced electron-phonon coupling [32]. After the discovery of superconductivity in bulk samples, thin films of BBPO were soon realized by different growth techniques, including sputtering [33–35] and pulsed laser deposition (PLD) [36].

Inspired by the discovery of a superconducting state at LAO/STO interfaces grown by PLD, we investigated BBO/BPO bilayers (BLs) in the expectation of identifying 2D superconductivity nonexistent in both parent compounds. Thin films of nominal $BaBi_{0.25}Pb_{0.75}O_3$, BBO, BPO, and BBO/BPO BLs were grown by PLD using commercially available, stoichiometric targets with purities of at least 99.9% at maximum reachable density. We used 5 mm $\times$ 5 mm single-crystalline (001)-oriented STO crystals as substrates, which we cleansed in acetone and isopropyl prior to deposition. HF buffering STO substrates [37,38] had no significant impact on the results. The deposition temperatures were $\approx$635 °C for $BaBi_{0.25}Pb_{0.75}O_3$ thin films and $\approx$552 °C for BBO, BPO thin films, and BBO/BPO BLs controlled by laser heating and monitored by pyrometers. The background pressure of pure oxygen was kept mass flow controlled at $\approx$1 mbar during growth. Our PLD system is equipped with a KrF laser with a fluency of $\approx$2 J/cm^2. We used laser pulse energies in the range of 550–750 mJ and laser pulse frequencies of 3–5 Hz.

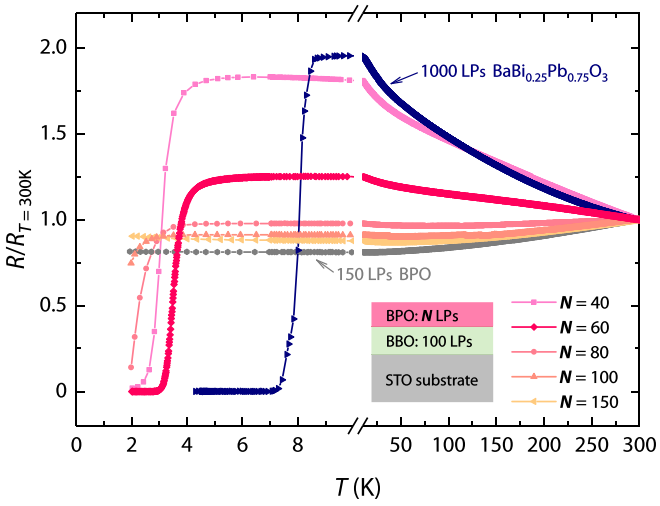

FIG. 1. Normalized resistances of pulsed-laser-deposition (PLD)-grown thin films of $BaPbO_3$ (BPO) and $BaBi_{0.25}Pb_{0.75}O_3$ and $BaBiO_3$ (BBO)/BPO bilayers (BLs) as a function of temperature. Whereas BBO thin films are highly insulating (not shown), BPO thin films show metallic behavior (gray hexagons). Thin films of nominal $BaBi_{0.25}Pb_{0.75}O_3$ are superconducting at low temperatures. BLs with a fixed thickness of BBO [100 laser pulses (LPs)] and variable thickness of the BPO top layer (controlled by the number N of LPs) undergo superconducting transitions (samples with $N = \{40, 60, 80, 100\}$).

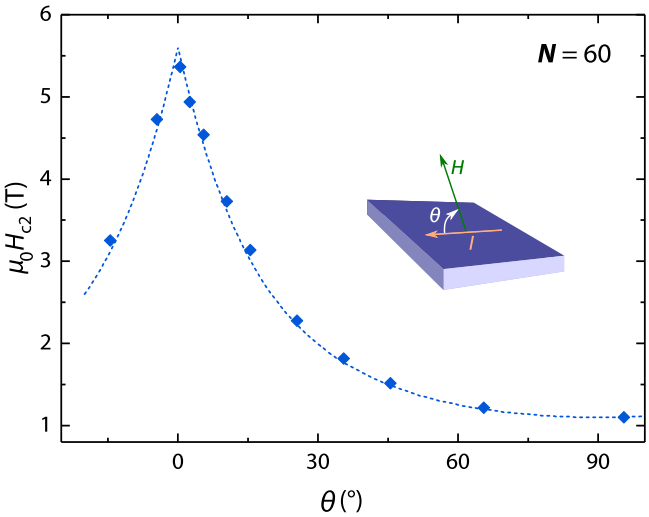

FIG. 2. Observed dependence of the upper critical magnetic field H_{c2} of a superconducting BL ($N = 60$) on the direction θ of the externally applied swept magnetic field (diamonds). The data are well represented by Eq. (1) (dashed line) which applies to a 2D superconducting sheet in the GL regime [40,41] with $H_{c2,\parallel} = 5.6\,\mathrm{T}$ and $H_{c2,\perp} = 1.1\,\mathrm{T}$.

After deposition the samples were cooled to ≈400 °C within 3 min and annealed at a background pressure of oxygen of ≈400 mbar for at least 17 min before the vacuum chamber was evacuated again.

For $BaBi_{0.25}Pb_{0.75}O_3$ thin films we used 1000 laser pulses (LPs), resulting in film thicknesses of ≈420 nm. For thin films of BBO and BPO we used 50–150 LPs, corresponding to film thicknesses of ≈25–75 nm for BBO and ≈17–50 nm for BPO. Concerning the BBO/BPO BLs we kept the thickness of the BBO starting layer constant (always 100 LPs) and varied only the number of LPs of the BPO top layer, denoted in the following by N.

All grown $BaBi_{0.25}Pb_{0.75}O_3$ thin films show an increase in resistance with decreasing temperature and a superconducting transition at $T_{c,ip} \approx 8\,\mathrm{K}$, which is determined at the inflection point (ip) of $R(T)$ at the transition (see Fig. 1, blue right-facing triangles). The lower T_c compared to that of bulk samples may be attributed to the steep dependence of T_c on the doping level [27].

BBO and BPO thin films grow smoothly, proved by frequent atomic force microscopy (AFM) analysis of their topography (see Supplemental Material [39], Fig. S1), and display peaks consistent with only (00l)-oriented planes in numerous x-ray diffraction (XRD) experiments. Transport properties were measured in common four-point geometry using copper wires attached by silver paste on the top layer of the unstructured samples to avoid degeneration of the BBO and BPO layers. Samples prepared in device structures using photolithography and ion etching qualitatively reproduce the $R(T)$ results of unstructured samples. BBO thin films are insulating, with resistances ranging from MΩ to GΩ over the whole accessible temperature range. Pure BPO thin films instead turn out to be metallic (see Fig. 1, gray hexagons).

BBO/BPO BLs reveal only peaks classified by (00l) orientation in XRD studies separated into individual reflexes for BBO and BPO. Peaks assigned to a homogeneously doped $BaBi_{1-x}Pb_xO_3$ phase could not be identified by XRD in any BL (see Supplemental Material [39], Fig. S2). BLs with $N = 30$ are semiconducting at all accessible temperatures; BLs with $N = 40$ show semiconductor-to-superconductor transitions with $T_{c,ip} \approx 3.0\,\mathrm{K}$ (see Fig. 1, pink squares). An increase in the BPO thickness ($N = 60$) shifts the superconducting transition temperature to values as high as $T_{c,ip} = 3.5\,\mathrm{K}$ (see Fig. 1, red diamonds). Interestingly, with a further increase in N we observe a reduction of the critical temperature ($N = \{80, 100\}$) and no superconducting transition for samples with $N = 150$. The observation of an optimal BPO thickness to reach maximum T_c and the suppression of superconductivity beyond this thickness allows for the assumption that the BL superconductivity is related to the interface (see below) and two-dimensional.

An estimate of the thickness of the present two-dimensional superconducting sheet can be retrieved by measuring the magnetotransport properties of our BLs. Such measurements are evaluated in the Ginzburg-Landau (GL) regime for magnetic fields up to H_{c2}.

Figure 2 exemplarily summarizes the observed dependence of the upper critical magnetic field H_{c2} of a BL with the number of LPs $N = 60$ on the angle θ, with respect to the sample plane of the externally applied swept magnetic field. As expected for a 2D superconductor, the in-plane field $H_{c2,\parallel}$ ($\theta = 0°$) is much higher than the out-of-plane field $H_{c2,\perp}$ ($\theta = 90°$) (see Fig. 2). Following Tinkham's analysis [40–42], both magnetic fields can be experimentally determined on the

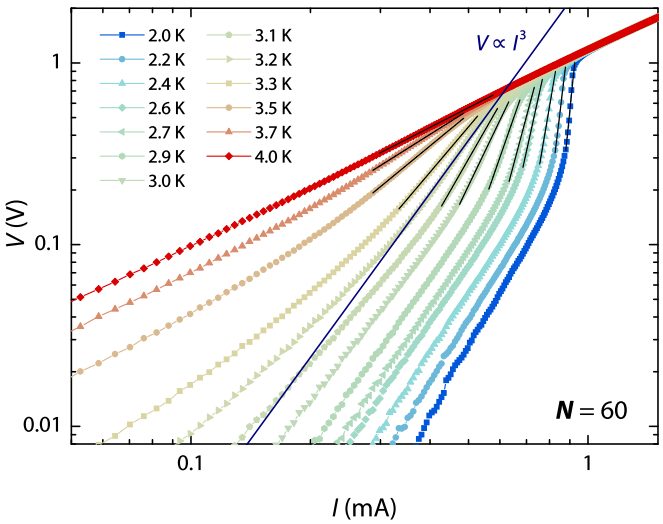

FIG. 3. Measured current-voltage (I-V) characteristics of a BBO/BPO BL ($N = 60$) at temperatures ranging from 2 K (blue) to 4 K (red). Straight black lines are polynomial fits following the measured data directly at the transition. At 3.2 K the I-V curve is best represented by a cubic fit (straight blue line) identifying 2D superconductivity following a Berezinskiĭ-Kosterlitz-Thouless (BKT) transition. The deviation of the fit for small currents is attributed to finite size effects [53].

basis of the relation

$$\left|\frac{H_{c2}(\theta)\sin\theta}{H_{c2,\perp}}\right| + \left(\frac{H_{c2}(\theta)\cos\theta}{H_{c2,\parallel}}\right)^2 = 1. \quad (1)$$

The GL theory for thin superconducting sheets allows us to express both magnetic fields in terms of the magnetic flux quantum ϕ_0, the thickness d_{sc} of the 2D superconducting sheet, the product of the penetration depth, and the thermodynamic critical field [43]. Eliminating the last quantity, the thickness d_{sc} can be calculated [42] with the help of experimentally obtained values of $H_{c2,\parallel}$ and $H_{c2,\perp}$ via

$$d_{sc} = \sqrt{\frac{6\phi_0 H_{c2,\perp}}{\pi H_{c2,\parallel}^2}}, \quad (2)$$

supporting a thickness of the 2D superconducting sheet of $d_{sc} \approx 11.8$ nm being clearly smaller than the nominal thickness of the BPO top layer. The calculated thickness d_{sc} is robust against different experimental determinations of H_{c2} (see Supplemental Material [39], Fig. S4). In contrast, for a thin film of nominal $BaBi_{0.25}Pb_{0.75}O_3$ (60 LPs) we calculate $d_{sc} \approx$ 26 nm, which is the same size as the overall thickness of the thin film of 25 nm (see Supplemental Material [39], Fig. S5).

The coherence length of the BL ($N = 60$) is estimated to be $\xi_{GL} \approx 11.0$ nm, a value we extracted from the temperature dependence of the upper critical magnetic field obtained from $R(T, H)$ measurements (see Supplemental Material [39], Fig. S6). The superconducting sheet thickness d_{sc} is therefore comparable to the GL coherence length ξ_{GL}, which is consistent with the prerequisites of the GL theory [44,45] identifying the observed superconductivity as two-dimensional.

If the superconducting transition is really caused by the interface, then a likely scenario is that the experimentally

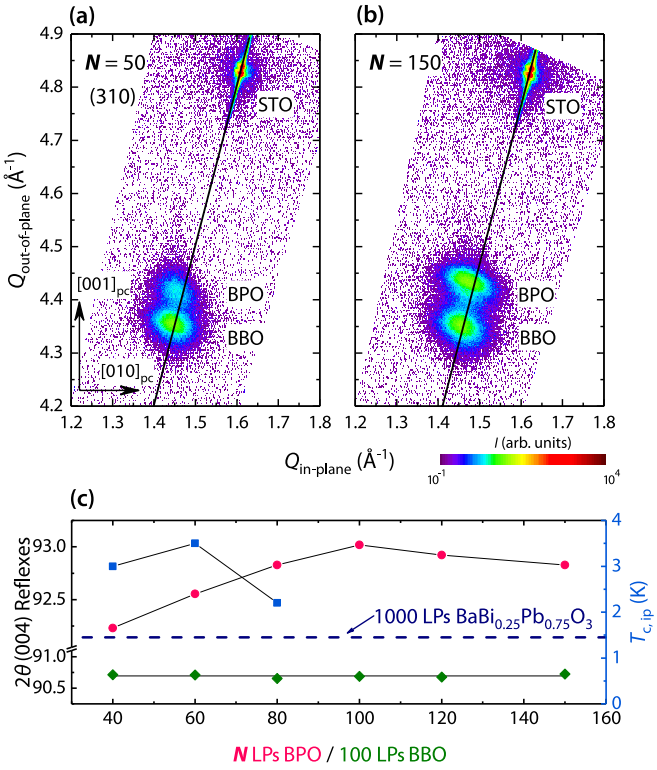

FIG. 4. XRD studies of BLs of BBO (100 LP)/BPO (N LP) grown on (001)-oriented STO substrates. Reciprocal space maps of BLs for (a) $N = 50$ (superconducting) and (b) $N = 150$ (metallic). Whereas BBO grows completely relaxed on STO substrates, following the relaxation line (black), the locations of both peaks of BPO are clear indicators for strained growth of BPO on BBO. The observed shift of the BPO peak away from BBO peak for larger N supports the idea that the concurrent observed changes in superconductivity are affected by strain. (c) Obtained (004) peak positions of BBO and BPO in BBO/BPO BLs from a series of $\theta/2\theta$ scans and critical temperatures for selected BLs (black lines serve as guides to the eye). Whereas BBO shows no significant shift in its peak positions, the BPO peaks move to lower angles with decreasing N, supporting ongoing strain-induced growth. This shift of the BPO peak is accompanied by the occurrence of superconductivity in the BLs (see blue squares and corresponding temperature axis on the right).

verified 2D superconducting sheet shows signatures of a BKT transition [46–50] identified by carefully examining the progression of current-voltage (I-V) characteristics taken at temperatures around T_c: the applied current I breaks vortex-antivortex pairs and yields at $T = T_{BKT}$ the well-known $V = I^\alpha$ behavior with $\alpha = 3$, whereas the voltage V responds linearly in I for a state with free vortices above T_{BKT} [51]. Direct validation of this observation can be done by analyzing the $R(T)$ dependence taken in four-point geometry. For a BKT transition, the resistance follows $R \propto R_n \exp(-b/\sqrt{t})$ [48] near T_{BKT}, with b being a material parameter on the order of unity [51] and $t = T/T_{BKT} - 1$. Interpreting our data in the context of a BKT transition yields $b = 1.22$ and $T_{BKT} = 3.26$ K, matching the value $T_{BKT} = 3.19$ K obtained independently from the I-V measurements (see Supplemental Material [39], Fig. S3). Below T_{BKT} two different nonlinear regimes are identified in the I-V characteristics of Fig. 3: for

small currents finite-size effects emerge that are expected to cause Ohmic behavior [52]. Yet it was argued more recently that a nonlinear I-V characteristic results from the unbinding of virtual vortex-antivortex pairs through vortices penetrating the edge of the sample [53]. The resulting non-Ohmic behavior is, in fact, observed for small currents. However, we also observe a crossover to a regime with a larger exponent α at higher currents (for fixed temperature at or below T_{BKT}) where the standard BKT behavior is established. We conclude that the finite-size effects [53] do not dominate the I-V characteristics for sufficiently large currents (where the fits in Fig. 3 are drawn in). The agreement of our transport data (see Fig. 3) with the BKT predictions together with our magnetoresistance evaluation signifies unambiguously that, indeed, a 2D superconducting sheet is formed within the BLs.

BBO/BPO BLs with different BPO top layer thicknesses show a variation not only of the critical temperature but also of the crystallographic properties. Reciprocal space maps, which were taken for BLs with $N = 50$ and $N = 150$ [see Figs. 4(a) and 4(b)], prove that BBO grows epitaxially and fully relaxed on STO substrates, consistent with domain-matched epitaxy [54,55]. BPO, however, grows strained on top of BBO for thin layers [$N = 50$, Fig. 4(a)] and relaxes more and more for thicker layers [$N = 150$, Fig. 4(b)]. We studied the strain effect in more detail in XRD $\theta/2\theta$ measurements taken for several BLs with different numbers of LPs N [see Fig. 4(c), green diamonds and red circles].

For BLs with $N = \{100,120,150\}$ the peak position of BPO is stable, serving as an indication for a relaxed state. With decreasing N the 2θ position of the (004) peak of BPO shifts towards smaller angles, supporting interface-induced epitaxial strain in the growing lattice of BPO on BBO accompanied by the observed arising 2D superconductivity [see Fig. 4(c), blue squares].

These observations aid the idea of the occurrence of 2D superconductivity being partly related to a strain effect emerging through the interface: as BLs with $N = 50$ become superconducting, whereas those with $N = 150$ stay metallic in the accessible temperature range, the possible intermittent existence of an established homogeneously doped region equal to $BaBi_{1-x}Pb_xO_3$ is hardly conceivable, as it also should show up in the XRD data, assuming its thickness is of the size of d_{sc}. Ultimately, a preferred thickness of the BPO film exists for assigning a robustly induced superconducting phase with maximum T_c.

In this study we have primarily shown that BLs of BBO and BPO become superconducting depending on the thickness of the BPO top layer with transition temperatures as high as $T_{\mathrm{c,ip}} = 3.5\,\mathrm{K}$ for our chosen layering of the BLs. Magnetotransport investigations provide evidence for the two-dimensionality of the superconducting sheet, estimating the thickness of the sheet to be $d_{\mathrm{sc}} \approx 11.8\,\mathrm{nm}$. Independently, the electrical transport characterization is compatible with a BKT transition emphasizing the 2D nature of the existing superconducting state within the BLs. X-ray studies suggest an epitaxial-matched strain effect at the interface between BBO and BPO accompanying the occurrence of the observed 2D superconducting state. The encountered transition in BBO/BPO bilayers is a remarkable further precedent of interface-driven ground-state variance. With the identification of a robust superconducting state at the interface of two "hidden" topological insulators [16] it will be compelling to determine the surface states of the superconducting sheet. There, we expect Majorana bound states at vortices [56] provided that gating [14] or chemical engineering [16] places the hidden Dirac cones at the Fermi level, so that a strong topological insulator is formed in proximity to the superconductor.

We thank A. P. Kampf for helpful discussions. We thank S. Esser for helpful discussions and his support in the measurement and the evaluation of the data for the reciprocal space maps. This work was supported by the DFG through TRR 80.

[1] J. Mannhart and D. G. Schlom, Science **327**, 1607 (2010).
[2] R. Hesper, L. H. Tjeng, A. Heeres, and G. A. Sawatzky, Phys. Rev. B **62**, 16046 (2000).
[3] S. Okamoto and A. J. Millis, Nature (London) **428**, 630 (2004).
[4] In fact, Hesper *et al.* [2] coined the term *electronic reconstruction* in connection with the surface electronic structure associated with a polar surface termination. Here we take the viewpoint of Okamoto and Millis [3], generalizing the term *electronic reconstruction* to include all situations where the surface or interface electronic phase differs from that in the bulk component materials.
[5] P. Zubko, S. Gariglio, M. Gabay, P. Ghosez, and J.-M. Triscone, Annu. Rev. Condens. Matter Phys. **2**, 141 (2011).
[6] A. Ohtomo and H. Y. Hwang, Nature (London) **427**, 423 (2004).
[7] A. Ohtomo and H. Y. Hwang, Nature (London) **441**, 120 (2006).
[8] M. Breitschaft, V. Tinkl, N. Pavlenko, S. Paetel, C. Richter, J. R. Kirtley, Y. C. Liao, G. Hammerl, V. Eyert, T. Kopp *et al.*, Phys. Rev. B **81**, 153414 (2010).
[9] N. Reyren, S. Thiel, A. D. Caviglia, L. Fitting Kourkoutis, G. Hammerl, C. Richter, C. W. Schneider, T. Kopp, A.-S. Rüetschi, D. Jaccard *et al.*, Science **317**, 1196 (2007).
[10] A. D. Caviglia, S. Gariglio, N. Reyren, D. Jaccard, T. Schneider, M. Gabay, S. Thiel, G. Hammerl, J. Mannhart, and J.-M. Triscone, Nature (London) **456**, 624 (2008).
[11] A. D. Caviglia, M. Gabay, S. Gariglio, N. Reyren, C. Cancellieri, and J.-M. Triscone, Phys. Rev. Lett. **104**, 126803 (2010).
[12] A. Gozar, G. Logvenov, L. Fitting Kourkoutis, A. T. Bollinger, L. A. Giannuzzi, D. A. Muller, and I. Bozovic, Nature (London) **455**, 782 (2008).
[13] D. Di Castro, C. Cantoni, F. Ridolfi, C. Aruta, A. Tebano, N. Yang, and G. Balestrino, Phys. Rev. Lett. **115**, 147001 (2015).
[14] B. Yan, M. Jansen, and C. Felser, Nat. Phys. **9**, 709 (2013).
[15] H. Ikushima and S. Hayakawa, Solid State Electron. **9**, 921 (1966).
[16] G. Li, B. Yan, R. Thomale, and W. Hanke, Sci. Rep. **5**, 10435 (2015).

[17] Here the term *hidden* is to be understood in the sense that the electronic structure displays a topological gap in the vicinity of the Fermi energy with a Dirac type of topological surface state [16].
[18] A. W. Sleight, US Patent No. 3,932,315 (1974).
[19] A. W. Sleight, Phys. C (Amsterdam, Neth.) **514**, 152 (2015).
[20] D. E. Cox and A. W. Sleight, Solid State Commun. **19**, 969 (1976).
[21] D. E. Cox and A. W. Sleight, Acta Crystallogr., Sect. B **35**, 1 (1979).
[22] C. M. Varma, Phys. Rev. Lett. **61**, 2713 (1988).
[23] H.-T. Kim, Phys. Rev. B **54**, 90 (1996).
[24] A. W. Sleight, J. L. Gillson, and P. E. Bierstedt, Solid State Commun. **17**, 27 (1975).
[25] T. D. Than, A. Koma, and S. Tanaka, Appl. Phys. **22**, 205 (1980).
[26] B. Batlogg, Phys. B (Amsterdam, Neth.) **126**, 275 (1984).
[27] E. Climent-Pascual, N. Ni, S. Jia, Q. Huang, and R. J. Cava, Phys. Rev. B **83**, 174512 (2011).
[28] P. Giraldo-Gallo, H. Lee, Y. Zhang, M. J. Kramer, M. R. Beasley, T. H. Geballe, and I. R. Fisher, Phys. Rev. B **85**, 174503 (2012).
[29] P. V. Balachandran and J. M. Rondinelli, Phys. Rev. B **88**, 054101 (2013).
[30] P. Giraldo-Gallo, Y. Zhang, C. Parra, H. C. Manoharan, M. R. Beasley, T. H. Geballe, M. J. Kramer, and I. R. Fisher, Nat. Commun. **6**, 8231 (2015).
[31] R. J. Cava, B. Batlogg, J. J. Krajeski, R. Farrow, L. W. Rupp, A. E. White, K. Short, W. F. Peck, and T. Kometani, Nature (London) **332**, 814 (1988).
[32] Z. P. Yin, A. Kutepov, and G. Kotliar, Phys. Rev. X **3**, 021011 (2013).
[33] L. R. Gilbert, R. Messier, and R. Roy, Thin Solid Films **54**, 129 (1978).
[34] M. Suzuki, T. Murakami, and T. Inamura, Jpn. J. Appl. Phys. **19**, L231 (1980).
[35] Y. Hidaka, M. Suzuki, T. Murakami, and T. Inamura, Thin Solid Films **106**, 311 (1983).
[36] S. V. Zaitsev-Zotov, A. N. Martynyuk, and E. A. Protasov, Sov. Phys. - Solid State **25**, 100 (1983).
[37] M. Kawasaki, K. Takahashi, T. Maeda, R. Tsuchiya, M. Shinohara, O. Ishiyama, T. Yonezawa, M. Yoshimoto, and H. Koinuma, Science **266**, 1540 (1994).
[38] G. Koster, B. L. Kropman, G. J. H. M. Rijnders, D. H. A. Blank, and H. Rogalla, Appl. Phys. Lett. **73**, 2920 (1998).
[39] See Supplemental Material at http://link.aps.org/supplemental/10.1103/PhysRevB.96.100507 for additional AFM images, x-ray characterizations, BKT evaluations and magnetotransport data.
[40] M. Tinkham, Phys. Rev. **129**, 2413 (1963).
[41] M. Tinkham, Phys. Lett. **9**, 217 (1964).
[42] F. E. Harper and M. Tinkham, Phys. Rev. **172**, 441 (1968).
[43] V. L. Ginzburg and L. D. Landau, Zh. Eksp. Teor. Fiz. **20**, 1064 (1950).
[44] M. Tinkham, *Introduction to Superconductivity* (McGraw-Hill, Hill, 1996).
[45] P. G. De Gennes, *Superconductivity of Metals and Alloys* (Westview Press, Boulder (Colorado), 1999).
[46] V. L. Berezinskiĭ, Zh. Eksp. Teor. Fiz. **59**, 907 (1970) [Sov. Phys. JETP **32**, 493 (1971)].
[47] V. L. Berezinskiĭ, Zh. Eksp. Teor. Fiz. **61**, 1144 (1971) [Sov. Phys. JETP **34**, 610 (1972)].
[48] J. M. Kosterlitz and D. J. Thouless, J. Phys. C **6**, 1181 (1973).
[49] J. M. Kosterlitz, J. Phys. C **7**, 1046 (1974).
[50] Estimated from $T_{\mathrm{BKT}} = 3.3$ K, our data yield a Pearl penetration depth of about 3 mm, which is comparable to the lateral size of our samples. We conclude that our samples are not too large for the observation of BKT behavior.
[51] B. I. Halperin and D. R. Nelson, J. Low Temp. Phys. **36**, 599 (1979).
[52] K. Medvedyeva, B. J. Kim, and P. Minnhagen, Phys. Rev. B **62**, 14531 (2000).
[53] A. Gurevich and V. M. Vinokur, Phys. Rev. Lett. **100**, 227007 (2008).
[54] T. Zheleva, K. Jagannadham, and J. Narayan, J. Appl. Phys. **75**, 860 (1994).
[55] J. Narayan and B. C. Larson, J. Appl. Phys. **93**, 278 (2003).
[56] L. Fu and C. L. Kane, Phys. Rev. Lett. **100**, 096407 (2008).